Author/s:
Ercole, F;Kim, C-J;Dao, NV;Tse, WKL;Whittaker, MR;Caruso, F;Quinn, JF

Title:
Synthesis of Thermoresponsive, Catechol-Rich Poly(ethylene glycol) Brush Polymers for Attenuating Cellular Oxidative Stress

Date:
2023-01-09

Citation:
Ercole, F., Kim, C. -J., Dao, N. V., Tse, W. K. L., Whittaker, M. R., Caruso, F. & Quinn, J. F. (2023). Synthesis of Thermoresponsive, Catechol-Rich Poly(ethylene glycol) Brush Polymers for Attenuating Cellular Oxidative Stress. BIOMACROMOLECULES, 24 (1), pp.387-399. https://doi.org/10.1021/acs.biomac.2c01211.

Persistent Link:
https://hdl.handle.net/11343/325331

# Synthesis of Thermoresponsive, Catechol-Rich Poly(ethylene glycol) Brush Polymers for Attenuating Cellular Oxidative Stress

*Francesca Ercole,[‡] Chan-Jin Kim,[†] Nam V. Dao,[‡,⁑] Warren K. L. Tse,[#] Michael R. Whittaker,[‡] Frank Caruso,[†] and John F. Quinn*[‡,#]*

‡ Drug Delivery, Disposition and Dynamics Theme, Monash Institute of Pharmaceutical Sciences, Monash University, Parkville, Victoria 3052, Australia

† Department of Chemical Engineering, The University of Melbourne, Parkville, Victoria 3010, Australia

⁑ Department of Physical Chemistry and Physics, Hanoi University of Pharmacy, Hanoi 10000, Vietnam

# Department of Chemical Engineering, Faculty of Engineering, Monash University, Clayton, Victoria 3800, Australia

*Correspondence to: john.f.quinn@monash.edu (J.F.Q.)

ABSTRACT

Herein, we report a platform to integrate customizable quantities of catechol units into polymers by reacting caffeic acid carbonic anhydride with polymers having pendant amine groups. Brush poly(ethylene glycol)–caffeamide (PEG–CAF) copolymers based on oligo(ethylene glycol)methyl ether methacrylate ($OEGMA_{500}$) were obtained with a catechol content of approximately 30, 40, and 50 mol% (vs OEGMA content). Owing to the hydrophobicity of the introduced CAF group, the catechol copolymers exhibited cloud points in the range of 23–46 °C and were used to fabricate thermoresponsive $Fe^{III}$ metal–phenolic network capsules. Polymers with the highest CAF content (50 mol%) proved most effective for attenuating reactive oxygen species levels in vitro, in co-cultured fibroblasts and breast cancer cells, even in the presence of an exogenous oxidant source. The reported approach to synthesize customizable catechol materials could be generalized to any amine-functional polymer, with potential biomedical applications such as adhesives or stimuli-responsive drug delivery systems.

KEYWORDS: Catechol-functionalized Polymer, Metal–Phenolic Networks, Thermoresponsive Polymer, Brush PEG, Capsules.

## INTRODUCTION

Catechols constitute a significant proportion of phenolic structures found in nature and exhibit diverse physicochemical properties.[1-6] Furthermore, catechols are known to have important functions in a range of biological processes.[7-9] For example, L-3,4-dihydroxyphenylalanine, a constituent of mussel proteins, is a key component in facilitating mussel adhesion to various substrates.[10-12] Catechols, including caffeic acid phenethyl ester,

are also key components in propolis, the resinous substance used by honeybees to secure their hives.[13] The ability of catechols to form strong and reversible bidentate coordination bonds with various metal ions, including $Cu^{II}$, $Zn^{II}$, and $Fe^{III}$, has also been exploited in synthetic contexts.[14-16] For instance, catechols have been used as coordinating ligands in the formation of metal–phenolic networks (MPNs), enabling the preparation of capsules with negligible cytotoxicity, tunable permeability, and with pH-responsive behavior.[17-19]

The range of chemical and physical interactions that catechols display continues to spur interest in catechol-functionalized polymers, in particular as structured and self-assembled materials.[20-25] It is anticipated that dynamic materials that can react to physical and chemical stimuli could emerge as a result of the synergistic combination of catechol and polymer properties.[26-30] Although there has been continuing focus on polymer structures modified with dopamine,[31] naturally derived phenolic acids, such as caffeic acid, represent attractive alternative starting materials for the preparation of phenolic polymers, particularly as they can be easily modified and do not readily undergo spontaneous oxidative self-polymerization under basic conditions (as does dopamine). Notably, caffeic acid can be readily isolated as a pure compound from numerous plant sources, such as coffee beans, making it an attractive source of catechol functionality.[32,33] Further, structures based on caffeic acid are known to exhibit antioxidant activity and therefore may potentially be applied toward preventing and/or mitigating oxidative stress and related diseases.[7,34,35] Thus, chemical strategies for integrating catechol functionality into polymers, in particular those that facilitate the incorporation of high and variable quantities, are important for the generation of new bioinspired catechol materials.

In the present work, we engineered a library of catechol-containing poly(ethylene glycol) (PEG) brush polymers via the reversible addition–fragmentation chain transfer (RAFT) copolymerization of oligo(ethylene glycol)methyl ether methacrylate ($OEGMA_{500}$). Having previously introduced a chemical strategy for attaching the catechol, caffeic acid, to a library

of amine-terminated, linear PEGs with different architectures (i.e., 2-, 4-, and 8-arm) and molecular weights (from 2.5 to 20 kDa),[27] in this work we expand the platform by applying the described catechol carbonic anhydride route to synthesize a PEG– caffeamide (CAF) conjugate with a higher catechol content. Furthermore the polymers featured pendant and randomly distributed units of oligo(ethylene glycol) methyl ether and catechols (CAFs), instead of a linear PEG backbone with terminal catechol groups, as well as increasing catechol contents of 30, 40, and 50 mol% (vs the OEGMA) content). The engineered brush PEG–CAFs displayed thermoresponsive behaviors, with associated cloud points in the range of 23–46°C that were strongly dependent on the catechol content. The brush PEG–CAFs were successfully applied as phenolic ligands to fabricate $Fe^{III}$ MPN capsules that underwent temperature-dependent size changes. Furthermore, inspired by the reported antioxidant properties of caffeic acid derivatives, the PEG–CAF building blocks, with variable catechol contents, were applied as macromolecular antioxidants using co-cultured cells which exhibit naturally elevated levels of reactive oxygen species (ROS).[36,37] Altogether, the reported methodology has enabled the preparation of biocompatible macromolecules with pendant and variable catechol content and demonstrates how catechol content can be exploited to manipulate a variety of important material properties.

## EXPERIMENTAL

**Materials.** Oligo(ethylene glycol) methyl ether methacrylate $M_n$ = ~500 g $mol^{-1}$ ($OEGMA_{500}$) and (2-boc-amino)ethyl methacrylate (BAEMA) were purchased from Sigma-Aldrich. $OEGMA_{500}$ was passed through a column of basic alumina to remove the inhibitor before use. A batch of BAEMA was purified by flash chromatography because of the presence of colored polymeric impurities. Initiators azobisisobutyronitrile (AIBN) and 1,1′-azobis(cyclohexanecarbonitrile) (ACHN) were purchased from Sigma-Aldrich. ACHN was used without purification and AIBN was purified by recrystallization from methanol before

use. The RAFT agent, 4-cyano-2-propyl benzodithioate (CPBDT), was purchased from Sigma-Aldrich at the highest purity available (>97% HPLC) and used as received. Hydrochloric acid 32% was purchased from Ajax Finechem. Solvents (excepting anhydrous solvents) were purchased from Merck Millipore and used as received. Trifluoracetic acid (TFA), triethylamine (TEA), *N*,*N*-dimethylformamide (DMF), dichloromethane (DCM), iron(III) chloride hexahydrate ($FeCl_3 \cdot 6H_2O$), 3-(*N*-morpholino)propanesulfonic acid (MOPS), and tetrahydrofuran (THF) were purchased from Merck Millipore (Burlington, MA, USA). Carboxylic acid-functionalized polystyrene (PS-COOH; 1.86 ± 0.03 μm) particles were purchased from microParticles GmbH (Berlin, Germany). Ultrapure water (18.2 MΩ cm), obtained from a three-stage Millipore Milli-Q plus 185 purification system (Millipore Corporation, Burlington, MA, USA), was used for all experiments. All other chemicals, such as reagents and anhydrous solvents, for synthesis were purchased from Sigma-Aldrich at the highest purity available and used without further purification (unless otherwise stated). A Reveleris flash chromatography system fitted with GRACE silica cartridges was used for the purification of monomers and intermediates. Thin-layer chromatography was performed on Merck silica $60F_{254}$ plates. (*E*)-3,4-Di-isobutoxycarbonyloxycinnamic mono-isobutyl carbonic anhydride (**iBocCAF**) and 4-arm, 10kDa linear, PEG–CAF **4a** were synthesized as per our previously reported protocol.[27]

Dulbecco's modified Eagle's medium – high glucose (DMEM) was purchased from Sigma-Aldrich. HEPES (4-(2-hydroxyethyl)-1-piperazineethanesulfonic acid buffer), DMEM with no phenol red (DMEM-NP), Dulbecco's phosphate buffered saline (DPBS), and fetal bovine serum (FBS) were obtained from Thermo Fisher Scientific. Trypsin 0.25% in ethylenediaminetetraacetic acid solution was received from Sigma-Aldrich and

penicillin/streptomycin (pen/strep, 10,000 units $mL^{-1}$ of penicillin and 10,000 μg $mL^{-1}$ of streptomycin) was purchased from Life Technologies. AlamarBlue cell viability reagent and CellROX Deep Red Reagent were obtained from Invitrogen. Rabbit anti-caveolin-1 antibody - caveolae marker (ab2910) and goat anti-rabbit IgG H&L (Alexa Fluor 488, ab150077) were purchased from Abcam. Goat serum was obtained from Sigma-Aldrich and paraformaldehyde (4%) in PBS was purchased from Santa Cruz Biotechnology (USA). Co-cultures of BJ-5ta and MCF-7 cells were plated on 96-well plates (Corning 96 Well Black Polystyrene Microplate, Sigma-Aldrich).

**Characterization and Analysis.** $^{1}H$ (400 MHz) and $^{13}C$ NMR (100 MHz) spectra were recorded on a Bruker UltraShield 400 MHz spectrometer at 25 °C running on the Bruker Topspin Software. Spectra were recorded for samples dissolved in deuterated chloroform ($CDCl_3$) or deuterated dimethyl sulfoxide ($d_6$-DMSO) and chemical shifts are reported as parts per million from external tetramethylsilane. Monomer conversions were obtained from the $^{1}H$ NMR spectra.

Gel permeation chromatography (GPC) was performed using a Shimadzu modular system comprised of a DGU-12A degasser, an SIL-20AD automatic injector, a 5.0 μm bead-size guard column (50 mm × 7.8 mm), three KF-805L columns (300 mm × 8 mm, bead size: 10 μm, pore size maximum: 5000 Å), an SPD-20A ultraviolet detector, and an RID-10A differential refractive index (RI) detector. The temperature of the columns was maintained at 40 °C using a CTO-20A oven. The eluent was *N,N*-dimethylacetamide (DMAc, HPLC grade, with 0.03% w/v LiBr) and the flow rate was kept at 1 mL $min^{-1}$ using a LC-20AD pump. A molecular weight calibration curve was obtained using commercial PS standards with a narrow molecular

weight distribution ranging from 500 to $2 \times 10^6$ g mol$^{-1}$. Polymer solutions at concentrations of approximately 2 mg mL$^{-1}$ were prepared and filtered through 0.45 μm filters prior to injection.

Scanning electron microscopy (SEM) analysis was conducted on a FlexSEM microscope (Hitachi, Japan). Atomic force microscopy (AFM) experiments were conducted on a NanoWizard II BioAFM instrument (JPK Instruments AG, Berlin, Germany) equipped with tapping-mode cantilevers.

Dynamic light scattering (DLS) measurements were conducted on a Malvern Zetasizer ZS series equipped with a 4 mW laser at $\lambda = 633$ nm and a detector angle of 173° running on DTS software. *Z*-average and polydispersity index values, illustrating the average diameters and size distribution, respectively, were determined via a cumulants analysis of the measured intensity autocorrelation function by the DTS software.

Cloud point temperature ($T_{CP}$) measurements were performed via UV–vis spectrophotometry. For the measurements, transmittance–temperature curves were generated to determine the $T_{CP}$ on a UV–vis spectrophotometer (Shimadzu UV-3600 UV–Vis–near-infrared) equipped with a circulation bath and a Peltier thermostat heating and cooling system. A 1 cm optical length cuvette with a screw-top lid was used. The sample was dissolved in deionized water and diluted to 5 mg mL$^{-1}$. The polymer solutions were heated and then cooled, with every measurement repeated at least twice.

**Cell Culture.** BJ-5ta human foreskin fibroblasts (CRL-4001) and MCF-7 breast cancer cells (HTB-22) were purchased from the American Type Culture Collection. Cells were grown in DMEM supplemented with 10% (v/v) FBS–1% (v/v) pen/strep and incubated at 37 °C in a humidified atmosphere containing 5% $CO_2$. Mycoplasma test was performed using the MycoAlert Detection Kit (Lonza) and was found to be negative.

**Co-Culture of Fibroblasts and Breast Cancer Cells.** The same culture conditions, as those from our previous work[36,37] were applied in the current study. When confluence reached 70–80%, cells were harvested by trypsinizing and were further suspended in DMEM–10% FBS–1% pen/strep and then plated on 96-well plates (100 μL media in each well). Each well contained a mixture of $0.2 \times 10^4$ BJ-5ta cells and $0.2 \times 10^4$ MCF-7 cells (co-culture), and in each experiment cells under different treatment conditions were seeded in triplicate. After 1 day, the medium was changed to DMEM with 1% FBS and 1% pen/strep (complete media), and the cells were maintained for another 3 days to achieve 70–80% confluence before subsequent experiments.

**Cell Viability Assay.** The toxicity of the polymers on the cells was evaluated using the AlamarBlue assay. Briefly, 4 days after plating, the medium was removed, and cells were treated with materials suspended in complete media. After 1 day, the media were aspirated and the cells were washed three times with DPBS to remove the unloaded materials. The AlamarBlue dye was employed at a dilution of 1:10 (v/v) in complete media. An aliquot (100 μL) of the dye-suspended media was added to each well, and after 2–4 h, the fluorescence intensity was measured on a CLARIOstar microplate reader using excitation and emission wavelengths of 530 and 590 nm, respectively. Cell viability (%) was obtained from the relative fluorescence intensity of treated wells compared to nontreated wells after subtracting the background. Triton X (0.1%) in complete media was used as the positive control for the AlamarBlue test (cell viability equals 0%).

**Reactive Oxygen Species Generation Detection.** Cells were treated with CellROX Deep Red Reagent (final concentration 5 μM) at 37 °C and 5% $CO_2$ for 50 min to allow the dye to be taken up. All unloaded dye was then removed, and cells were washed three times with DMEM-NP. The cells were subsequently analyzed using an Operetta High content imaging system (PerkinElmer, Glen Waverley, Australia) with an Olympus LUCPlanFLN 20× (NA

0.45) objective and an annexin V ac filter set (excitation 630/20 nm and emission 705/55 nm). Harmony software version 4.8 was used to collect and analyze the data. The differences in the brightfield values between the fibroblasts and breast cancer cells in the digital phase contrast channel were used to integrate the intracellular ROS levels for each cell type, with the aid of the PhenoLOGIC machine-learning functions equipped in the Harmony software. ROS generation was calculated based on intensity per cell per well after subtracting the background. To compare the effectiveness of different polymers, the materials were treated to the co-cultured cells in the same set of experiments (testing in parallel).

**Imaging.** Images were obtained using an Operetta high content imaging system (PerkinElmer, Glen Waverley, Australia) with an Olympus LUCPlanFLN 20× (NA 0.45) objective, using Harmony software version 4.8. The digital phase contrast channel was used to detect and distinguish the two cell lines for subsequent determination of the intensity for the individual cell lines as reported previously.[36] For each cell line, the final results show the average intensity of fluorescence per cell per well after subtracting the background.

All the data were generated from at least three independent experiments each comprising three technical replicates, and are presented as the mean ± standard error of the mean. For analysis of statistical variation among groups, tests were conducted in parallel in each experiment and a paired *t*-test or matched analysis of variance (ANOVA) was employed to analyze the differences.[38] All graphs were prepared and statistical analyses were conducted using GraphPad Prism (8.0.2), with reference to the Prism 8 Statistics Guide. Representative high-content fluorescence images used for probing the cellular ROS levels of co-cultured cells BJ-5ta and MCF-7, with a description of the method applied, are displayed in the Supporting Information.

**Synthesis of P(OEGMA)$_x$-*co*-P(BAEMA)$_y$, 1a–1c.** A typical copolymerization procedure for OEGMA$_{500}$ and BAEMA is as follows: The polymerization was carried out using the

following stoichiometry of $[CPBDT]_0$:$[OEGMA]_0$:$[BAEMA]_0$:$[AIBN]_0$ = 1:25:10:0.10, where $[CPBDT]_0$:$[Monomers]_0$ = 1:35 and $[OEGMA]_0$:$[BAEMA]_0$ = 24.5:10.5 (70:30), which describes the molar feed ratios used for **1a**. $OEGMA_{500}$ (1 g, $2.0 \times 10^{-3}$ mol), BAEMA (200 mg, 0. $86 \times 10^{-3}$ mol), CPBDT RAFT agent (18.1 mg, $8.16 \times 10^{-5}$ mol), AIBN (1.34 mg, $8.16 \times 10^{-6}$ mol), and toluene (2.3 mL) were placed in an 8 mL vial along with a magnetic stirrer bar and capped with a rubber septum. The reaction mixture was deoxygenated for 20 min by sparging with $N_2$. The deoxygenated mixture was placed in a preheated oil bath at 70 °C and the reaction mixture was left to stir for 6 h. The resulting mixture was then allowed to cool in an ice bath for ~15 min to terminate the polymerization and then exposed to air. The overall monomer conversion was determined by $^1$H NMR spectroscopy. The resonances of the vinyl peaks at 5.4 and 5.9 ppm (monomer only) and the $OCH_2$– peaks at 3.8–4.1 ppm (monomer and polymer) were integrated to obtain the conversions for the OEGMA and BAEMA polymerizations. Multiple precipitation and centrifugation steps (6×), using petroleum spirits 40–60 °C/diethyl ether (7:3, v/v) as the precipitant, were carried out to remove all traces of unreacted monomer. Residual solvent was then removed by blowing a gentle stream of air overnight. The final product, $P(OEGMA)_{21}$-*co*-$P(BAEMA)_9$-S-C=S-Ph **1a** was analyzed by $^1$H NMR spectroscopy and GPC. The $^1$H NMR spectra of the RAFT-terminated polymers, with main peak assignments, are provided in Figures S1–S3. The polymerization reagent quantities used for each polymer synthesis are listed in Table S1. The polymerization characteristics of the polymers functionalized with a RAFT end group are presented in Table S2.

**RAFT End Group Removal from $P(OEGMA)_x$-*co*-$P(BAEMA)_y$-S-C=S-Ph, 1a–1c.** A typical RAFT end group removal procedure is as follows: A solution of $P(OEGMA)_{21}$-*co*-$P(BAEMA)_9$-S-C=S-Ph **1a** (0.930 g, $7.3 \times 10^{-5}$ mol, 1 equivalent), 1-ethylpiperidine hypophosphite (EPHP) (0.071 g, $4.0 \times 10^{-4}$, ~5 equivalents), ACHN (5.8 mg, $2.4 \times 10^{-5}$, 0.33 equivalents), and dioxane (4.7 mL) were added to a 20 mL reaction vessel with a magnetic

stirrer bar, and the vessel was capped with a rubber septum. The reaction mixture was deoxygenated with $N_2$ for 20 min and then placed into a preheated oil bath at 100 °C with stirring for 2 h. The radical-induced reduction process was terminated by placing the sample in an ice bath for 15 min. The product was then recovered by multiple precipitations into diethyl ether/petroleum spirits 40–60°C (1:3, v/v). After drying under a stream of $N_2$, the removal of the thiocarbonylthio end group was determined to be only 90% by $^1$H NMR spectroscopy. The procedure was therefore repeated 2 more times, as described above, with no work up in between. After terminating the reaction, the product was precipitated into diethyl ether/petroleum spirits 40–60°C (1:3, v/v) and dried under a stream of air. To remove reaction by-products from EPHP, most likely salts, the polymer was dissolved in chloroform and washed successively with water and brine. The chloroform solution was then dried with $MgSO_4$, filtered and the chloroform was then removed under vacuum. The decolorized polymer was analyzed by GPC and $^1$H NMR spectroscopy, which showed that the RAFT end groups and reaction by-products had been adequately removed. Specifically, three distinct signals in the $^1$H NMR spectrum ($\delta$ 7.35, 7.50, and 7.90 ppm), representing the aromatic benzodithioate, were absent. The extent of RAFT removal was assessed by comparing the UV detector signal at 310 nm with respect to the RI detector signal, both before and after the reduction reaction. The GPC results for each polymer are displayed in Table S3.

**Synthesis of P(OEGMA)$_x$-*co*-P(iBocCAF)$_y$-*co*-P(iBocC)$_z$ (2a–2c) from 1a–1c.** A typical iBocCAF conjugation procedure is as follows: Polymer **1a**, with RAFT end group removed, P(OEGMA)$_{21}$-*co*-P(BAEMA)$_9$-H, was weighed into a vial (400 mg, $3.4 \times 10^{-5}$ mol polymer, ~$3.1 \times 10^{-4}$ mol Boc-protected amine side groups) and dissolved in dry DCM (1.5 mL). A magnetic stirrer bar was added and the solution was stirred until complete dissolution. To the solution, TFA was added dropwise (1.5 mL), the vial was capped, and the solution left to stir for 4 h. Then, a large amount of DCM/TFA was removed with a stream of air, with further

removal achieved under vacuum. A small sample was retrieved and monitored for complete Boc deprotection by $^1$H NMR spectroscopy. Completion of the deprotection reaction was indicated by the complete disappearance of the *tert*-butyl peak in the $^1$H NMR spectrum at ~1.5 ppm measured in $CDCl_3$ solvent.

After drying the sample under vacuum and capping the reaction vessel, the polymer was redissolved in dry DCM (2 mL) and kept under $N_2$. In a separate vial, iBocCAF was added (210 mg, $4.35 \times 10^{-4}$ mol), followed by dry DCM (2.0 mL). The solution was kept stirring under $N_2$. The solution of polymer (Boc-deprotected, TFA-amine salt) was stirred under a gentle stream of $N_2$ and cooled in an ice bath. To neutralize the pendant TFA salts, TEA was added dropwise using a syringe (90 μL, $6.4 \times 10^{-4}$ mol, 2 equivalents vs TFA salt). A vent needle was temporarily added to the vial to release any fumes. The polymeric solution was then taken up into a syringe and slowly added dropwise to the solution of iBocCAF, while cooling the reaction vessel in an ice bath. After addition was complete, the solution was left to react (stirring) over ice and $N_2$ for 1 h and then left to equilibrate to ambient temperature overnight. The solution was then concentrated to half its original volume and then added dropwise into excess diethyl ether:petroleum spirits 60–80 °C (1:4 v/v) to precipitate the product, P(OEGMA)$_{21}$-*co*-P(iBocCAF)$_8$-*co*-P(iBocC)$_2$ **2a** as a sticky clear residue. Precipitation was carried out thrice to remove excess iBocCAF. To remove residual TEA-TFA salts, as evidenced by $^1$H NMR spectroscopy, the polymerization solution was transferred to a dialysis tubing (nominal molecular weight cutoff 3500) and dialyzed against acetone, with at least 5 exchanges of solvent. Acetone was then removed under vacuum and residual solvent was then removed by blowing a gentle stream of air over the polymer residue overnight (mass yield: ~90%). Each polymer was analyzed by $^1$H NMR spectroscopy and GPC. The $^1$H NMR spectra of the iBoc-protected caffeamide PEG brush polymers, P(OEGMA)$_x$-*co*-P(iBocCAF)$_y$-*co*-P(iBocC)$_z$ (**2a–2c**), with main peak assignments are shown in Figures S4–S6. The reagent quantities used for

each conjugation reaction are listed in Table S4 and characteristics of polymers are presented in Table S5.

**Synthesis of P(OEGMA)$_x$-*co*-P(CAF)$_y$-*co*-P(iBocC)$_z$ (3a–3c) from 2a–2c.** A typical isobutyl carbonate deprotection procedure is as follows: P(OEGMA)$_{21}$-*co*-P(iBocCAF)$_8$-*co*-P(iBocC)$_2$ **2a** (360 mg, $2.4 \times 10^{-5}$ mol) was dissolved in dry DCM (1.8 mL) in a vial and kept under $N_2$. To this solution was added TEA (121 μL, $8.8 \times 10^{-4}$ mol) as a sacrificial counter base for the catechols. In a separate vial, a 33% v/v solution of isopropylamine (IPAM) was prepared in dry DCM (1500 μL of IPAM in 3.0 mL DCM, 4.07 M). The solution was cooled in an ice bath and then deoxygenated with $N_2$ for 15 min. An aliquot (1067 μL) of the IPAM/DCM solution was then transferred dropwise to the polymer solution (containing **2a**, TEA, and DCM), and the resulting solution was cooled and stirred. The final concentration of IPAM in DCM was ~12% v/v (~1.5 M) which is approximately 20 equivalents of IPAM per isobutyl carbonate-protected catechol (iBocCAF group). The solution was stirred for 16 h at ambient temperature under $N_2$. The yellow solution was then concentrated to half its original volume and added dropwise to excess diethyl ether:petroleum spirits 60–80°C (1:4 v/v) to precipitate the product, P(OEGMA)$_{21}$-*co*-P(CAF)$_8$-*co*-P(iBocC)$_2$ **3a**, as a sticky tan residue. The solid was then dissolved in 0.1 M HCl buffer and dialyzed against acidic water for 3 days. The product was then freeze dried to isolate the product as a tan residue (yield: ~80%). The $^1$H NMR spectra of the caffeamide PEG brush polymers, P(OEGMA)$_x$-*co*-P(CAF)$_y$-*co*-P(iBocC)$_z$ (**3a–3c**), with main peak assignments are shown in Figures S9–S11. The characteristics of the polymers are shown in Table S5 and reagent quantities used for each deprotection reaction are listed in Table S6.

**Assembly of Brush PEG–CAF−Fe$^{III}$ MPN Capsules.** The capsules were prepared as follows: A suspension (50 μL) of PS-COOH particles (1.86 ± 0.03 μm, 100 mg mL$^{-1}$) was transferred to a 1.7 mL microcentrifuge tube and washed twice with water. The PS-COOH

particles were washed with water by vortexing and sonication for 1–2 min and then pelleted by centrifugation (2000*g*, 2 min). The supernatant was then discarded, and the process was repeated. A stock solution containing brush PEG–CAF copolymer and $FeCl_3 \cdot 6H_2O$ was added to the particle suspension to obtain final concentrations of 0.5 and 1 mM, respectively, and the mixture was vortexed for 2 min. The final concentration of the PS-COOH particles was 10 mg $mL^{-1}$. MOPS buffer (25 mM, pH 7.4, 0.7 mL) was then added to raise the pH above 7, leading to the formation of bis- and tris-coordination complexes between brush PEG–CAF copolymer and $Fe^{III}$ ions. After increasing the pH, excess and unreacted materials were removed by pelleting the particles (2000*g*, 2 min) and the supernatant was discarded. The resulting MPN-coated particles were washed three times with water (500 μL) by repeated centrifugation (2000*g*, 2 min) and redispersion. The particles were then resuspended in water (50 μL), and THF (1 mL) was added to remove the template particles. After 1 h, the MPN capsules were pelleted through centrifugation (2000*g*, 2 min) and washed with THF (500 μL) five times. At the final THF washing step, the capsules were pelleted through centrifugation (2000*g*, 3 min) and the supernatant was discarded. The resulting brush PEG–CAF−$Fe^{III}$ MPN capsules were washed with water once and then resuspended in water (300 μL).

**Size Change of MPN capsules as a function of pH and temperature.** To examine the pH-dependent size changes of the MPN capsules, the capsules were diluted with 50 mM MOPS buffer (10 mM final concentration, pH 3, 5, 7, or 9) and the size measured by DLS at 25 °C. To examine the thermally-induced size changes of the capsules, PEG–CAF−$Fe^{III}$ MPN capsules were first dispersed in water. The temperature-dependent size changes of the capsules were then monitored by DLS at 25–50 °C with 10 min equilibration time at each temperature.

## RESULTS AND DICUSSION

**Design and Synthesis of Catechol-Functionalized Brush PEG.** The coupling chemistry applied in this work involves the use of the mixed carbonic anhydride of caffeic acid, which is

formed by reacting caffeic acid with isobutyl chloroformate (Scheme 1a). In this structure, both hydroxyls of the catechol moiety are acyl-protected as isobutyl carbonate groups, while the carboxylic acid is activated as the carbonic anhydride to permit reaction with amine. The reaction of the carbonic anhydride with polymeric amines yields the corresponding iBoc-protected caffeamide. Deprotection of the isobutyl carbonate groups, to yield catechols, is achieved using an excess of small molecule amine. In previous work,[27] this methodology afforded a library of multiarm linear PEG–CAF building blocks, such as the 10 kDa 4-arm PEG−CAF, referred to herein as **4a** (Scheme 1b).

As a more versatile alternative to targeting terminal amines, in the present work we synthesized polymers with side-functional amines. These were generated from a library of boc-protected amine side-functional polymers, P(OEGMA)$_x$-*co*-P(BAEMA)$_y$, obtained via RAFT polymerization of OEGMA$_{500}$ with the co-monomer BAEMA (Scheme 2a). The polymers were each analyzed by $^1$H NMR spectroscopy and GPC (Tables S1 and S2 and Figures S1–S3). After $^1$H NMR elucidation of the composition and number average molecular weight ($M_n$), the thiocarbonylthio end groups were removed from the polymers by radical-induced reduction using EPHP and ACHN initiator, as confirmed by GPC with UV detection (Table S3). This step was necessary to avoid aminolysis of the thiocarbonylthio end groups during the final deprotection step, which otherwise would generate reactive thiols. The P(OEGMA)$_x$-*co*-P(BAEMA)$_y$ polymers **1a–1c** were formulated to contain approximately 30, 40, and 50% of protected amines vs the OEGMA content, which was maintained at a target degree of polymerization value of 20×OEGMA$_{500}$ units. Specifically, for the ROS comparison study, we aimed to have an $M_n$ value of PEG in the brush polymers equivalent to that of **4a**, i.e., $M_n$ of ~10 kDa.

**Scheme 1. (a) Synthesis of caffeic acid carbonic anhydride (iBocCAF) from caffeic acid. Reaction conditions: (i) isobutyl chloroformate, *N*-methylmorpholine, THF, −15 °C. (b)**

**Structure of 4-arm, 10kDa linear PEG–CAF, 4a, prepared from iBocCAF and 4-arm PEG amine 10kDa.**

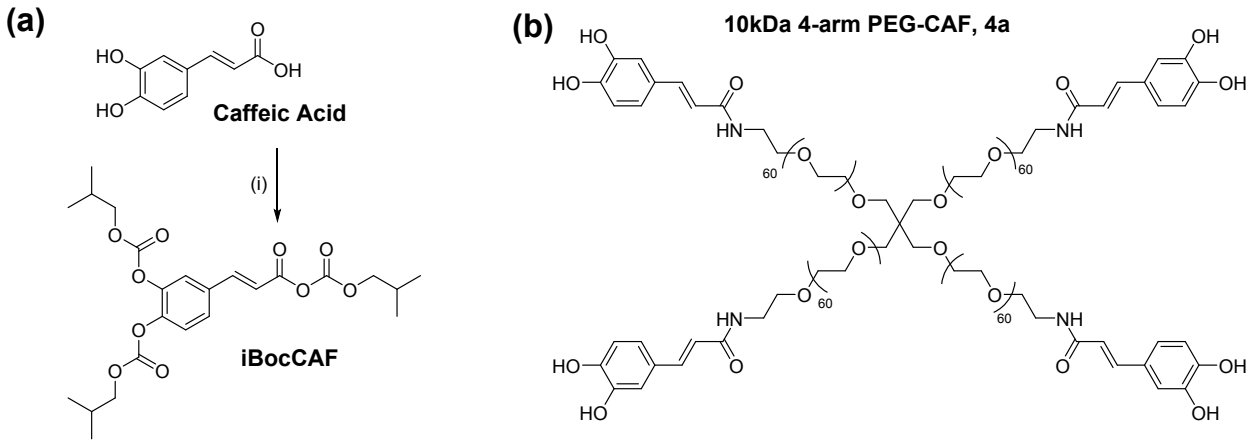


**Scheme 2. Synthesis of RAFT-derived catechol side-functionalized PEG brush polymers, P(OEGMA)$_x$-*co*-P(CAF)$_y$-*co*-P(iBocC)$_z$, prepared using the caffeic acid carbonic anhydride method.[a] Reaction conditions: (i) toluene, AIBN, 70 °C, 5–6 h; (ii) EPHP, ACHN, dioxane, 100 °C, 2 h (2×); (iii) TFA/DCM, TEA; (iv) iBocCAF (displayed in Scheme 1), DCM, 0 °C → room temperature, overnight (curved arrows indicate two possible sites of attack by amines); and (v) IPAM, DCM, overnight, room temperature.**

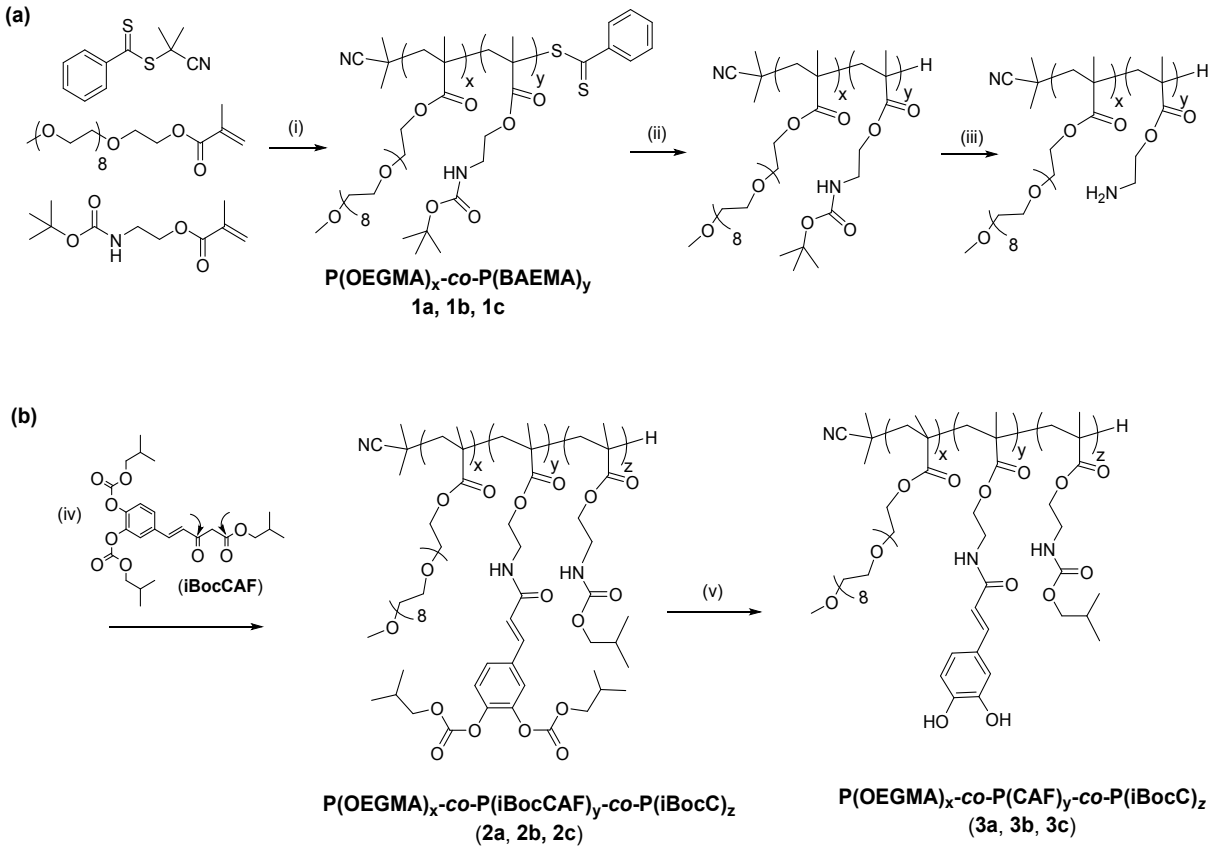


[a] As a result of removal of RAFT end group and overlapping $^1$H NMR peaks, the composite quantities ($x$, $y$, and $z$) are provided as estimates only. For P(OEGMA)$_x$-*co*-P(BAEMA)$_y$ **1a**: $x$ = 21, $y$ = 9; **1b**: $x$ = 22, $y$ = 16; and **1c**: $x$ = 20, $y$ = 20. For P(OEGMA)$_x$-*co*-P(iBocCAF)$_y$-*co*-P(iBocC)$_z$ **2a**: $x$ = 21, $y$ = 8, $z$ = 2; **2b**: $x$ = 22, $y$ = 16, $z$ = 3; and **2c**: $x$ = 20, $y$ = 19, $z$ = 5. For P(OEGMA)$_x$-*co*-P(CAF)$_y$-*co*-P(iBocC)$_z$ **3a**: $x$ = 21, $y$ = 8, $z$ = 2; **3b**: $x$ = 22, $y$ = 16, z = 3; and **3c**: $x$ = 20, $y$ = 19, $z$ = 5.

Boc deprotection of the P(OEGMA)$_x$-*co*-P(BAEMA)$_y$ polymers and subsequent neutralization of the amine trifluoroacetic acid salt was followed by coupling of iBocCAF with amine side groups (Scheme 2b). This was performed in DCM by mixing the solutions of iBocCAF and polymeric amine with some initial cooling, affording the iBoc-protected caffeamide side-functionalized PEG brush polymers, i.e., P(OEGMA)$_x$-*co*-P(iBocCAF)$_y$-*co*-P(iBocC)$_z$ **2a**–**2c**. In this step, amide bond formation occurs via the reaction of the amine with the caffeic acid carbonyl of iBocCAF, with a loss of $CO_2$ and isobutanol (Scheme S1, step 1). The protected caffeamide PEG brush polymers were isolated by precipitation in diethyl ether

and petroleum spirits and analyzed by both $^1$H NMR spectroscopy and GPC before deprotection (Figures S4–S6, Tables S4 and S5).

As noted in our previous work,[27] a carbamate side product can form upon reaction of the amine with carbonate groups of the carbonic anhydride during the coupling step, yielding isobutyl carbamate side groups instead of iBoc-protected caffeamide functionality (as described in Scheme S2). This side reaction is thought to be influenced by the nature of the amine (i.e., primary or secondary), temperature, and solvent.[39] To identify and quantify the proportion of side-product functionalization in the final product by $^1$H NMR spectroscopy, a brush PEG–carbamate control polymer was synthesized, P(OEGMA)$_{20}$-*co*-P(iBocC)$_{20}$ (Figures S7 and S8). As noted previously, using an excess of iBocCAF during the coupling step (1.3–2 equivalents vs amine) minimizes the formation of the carbamate side product. The side functionality was found to account for approximately 5–10% of the total final polymer composition (as shown in Table S5).

In the next step, a low-molecular weight amine (IPAM) was used to deprotect the carbonate groups, releasing a small-molecule carbamate via the reaction of the amine with isobutyl carbonate groups (Scheme S2, step 2). The carbamate was extracted from the polymer mixture by precipitation, followed by dialysis to remove trace amounts. For each polymer, a large excess of amine was added to completely deprotect the isobutyl carbonate groups, yielding catechol side-functionalized PEG brush polymers P(OEGMA)$_x$-*co*-P(CAF)$_y$-*co*-P(iBocC)$_z$ **3a–3c**. The final polymers were analyzed by $^1$H NMR spectroscopy (Figures S9–S11) and GPC (Table S5).

The GPC traces for the deprotected catechol-functionalized polymers were somewhat broader than those measured in the previous step, with dispersity indices of 1.5–2.1. This broadening could potentially be attributed to the sticking or adsorption of the polymers on the column due to the presence of numerous catechol hydroxyl groups. However, a notable high

molecular weight shoulder was also observed in each trace. This could likely be due to the occurrence of oxidative coupling reactions although the polymers remained fully soluble and did not take on the dark color of a highly oxidized product. An increase in yellow–brown coloration is thought to be qualitative evidence of oxidative coupling, which could manifest as branching and crosslinking reactions.[40] By deconvoluting each of the GPC traces (as in Figure S12), the high molecular weight shoulder was found to account for 10–20% of the total area of the peaks. Furthermore, the derived peak molecular weight (the $M_p$ value), corresponding to the high molecular weight shoulder, was found to be approximately three times the value of the main peak in the GPC traces. This supports the idea that the brush PEG–CAF polymers undergo some branching reactions due to oxidative coupling. This could occur during GPC analysis or the deprotection step, and unlikely to occur exclusively in either setting. When the deprotection step was performed without degassing the amine stock solution, the polymers darkened more substantially, indicating that oxidation is a likely side reaction during this step. However, taking into consideration the soluble nature of the polymers and the analogous aromatic proton resonances in each $^1$H NMR spectrum, this would suggest that oxidative coupling was not extensive.

Interestingly, the catechol side-functionalized PEG brush polymers were found to be fluorescent, as has been noted in literature for caffeic acid.[41] Figure S13 displays the fluorescence spectra of **3c** and caffeic acid in water. Due to the low excitation (310 nm) and emission wavelengths (420 nm) and potential photo-reactivity of caffeic acid derivatives[42], the application of this inherent fluorescence in imaging applications was not investigated.

**Thermoresponsive Behaviors of 3a–3c.** Despite the possible occurrence of branching, the brush PEG–CAF polymers **3a**–**3c** were completely soluble in a range of organic solvents (chloroform, DCM, DMAc, DMSO, DMF). The brush PEG–CAF polymer **3a** also dissolved in water but in contrast, dissolution of **3c** in water did not occur at room temperature, especially

at concentrations ≥1.0 mg $mL^{-1}$, while sample **3b** only sparingly dissolved in water even with prolonged agitation. Dissolution of **3b** and **3c** could only be initiated by cooling the samples to below 5 °C but re-warming the solutions caused them to phase separate again. These observations were indicative of lower critical solution temperature (LCST) behavior displayed by the brush PEG–CAF polymers. For polymer mixtures, heating above the LCST typically results in a transition from a coil to a globule, whereby the components are no longer miscible, resulting in cloudiness and precipitation of the polymer with increasing temperature.[43] The unexpected thermoresponsive behavior of **3a–3c** was further probed by measuring the $T_{CP}$ of the polymers. UV–Vis spectrophotometry was employed, in which the transmittance, derived from the absorbance value at 500 nm, is measured as a function of temperature. The $T_{CP}$ is broadly thought of as the temperature at which phase separation starts and the solution becomes turbid/cloudy under a given set of conditions, such as heating rate and concentration. However, as there is no broadly accepted agreement on which point of the transmittance–temperature curve should be taken as the $T_{CP}$ for polymer–water mixtures, we used the inflection point in accordance with the literature.[44] The inflection point was determined as the minimum value of the first derivative of the transmittance–temperature curves (Figure S14). As observed in Figure 1a, the brush PEG–CAF polymers displayed $T_{CP}$ values that were dependent on their catechol content. Given that the P(OEGMA) content in each copolymer was kept relatively the same (~10 kDa, ~20 units), the caffeamide side functionality is the likely reason for the observed changes in thermal response.

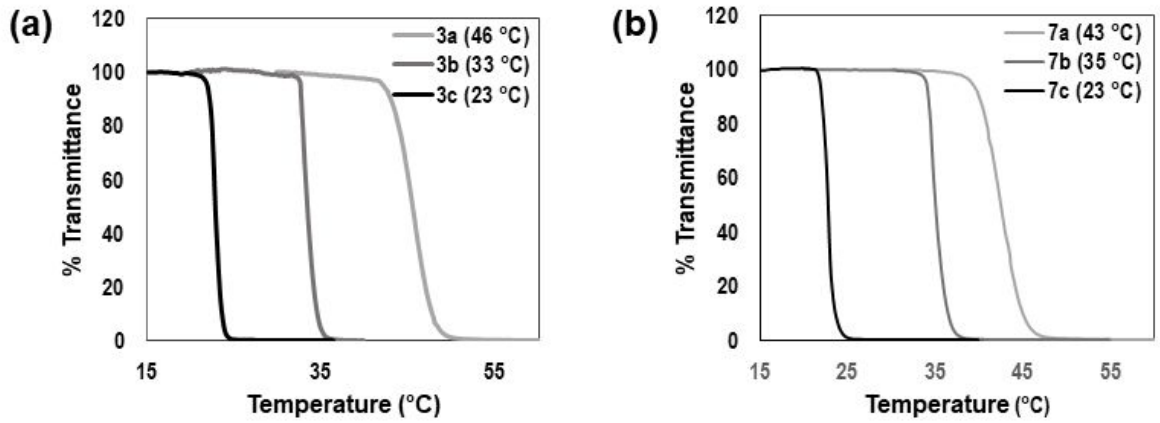


**Figure 1.** Transmittance–temperature curves of the brush PEG–CAF polymers (a) P(OEGMA)$_{21}$-*co*-P(CAF)$_8$-*co*-P(iBocC)$_2$ (**3a**), P(OEGMA)$_{22}$-*co*-P(CAF)$_{16}$-*co*-P(iBocC)$_3$ (**3b**), and P(OEGMA)$_{20}$-*co*-P(CAF)$_{19}$-*co*-P(iBocC)$_4$ (**3c**); and (b) replicate batches P(OEGMA)$_{20}$-*co*-P(CAF)$_8$-*co*-P(iBocC)$_2$ (**7a**), P(OEGMA)$_{20}$-*co*-P(CAF)$_{15}$-*co*-P(iBocC)$_3$ (**7b**), and P(OEGMA)$_{21}$-*co*-P(CAF)$_{22}$-*co*-P(iBocC)$_5$ (**7c**). The $T_{CP}$ values are presented in parentheses (conditions: 0.5 wt% in water, 0.5 °C min$^{-1}$ heating rate with 1 min equilibration, absorbance monitored at 500 nm wavelength).

To further confirm the thermoresponsiveness of the brush PEG–CAF polymers **3a**–**3c**, we synthesized a replicate batch, **7a**–**7c**, using the same synthetic protocol (Scheme S3, Tables S7–S11). The intermediate (**5a**–**5c**, **6a**–**6b**) and final polymers (**7a**–**7c)** were analyzed by $^1$H NMR spectroscopy (Figures S15–S23) and GPC (Table S12). The replicate batch showed the same trend in thermal behavior as **3a**–**3c**, as well as similar $T_{CP}$ values with respect to their compositions (Figure 1b and Figure S24).

Poly(*N*-isopropylacrylamide), P(NIPAM), is the most widely investigated thermoresponsive polymer in literature exhibiting an LCST of ~32 °C in water.[45,46] However, OEGMA and oligo(ethylene glycol acrylate) (OEGA)-based polymers, are also known to display LCST behaviors and have become viable alternatives to P(NIPAM) as they combine the advantages of PEG, namely biocompatibility, low immunogenicity, and thermoresponsiveness, in a single

building block.[47,48] A common strategy to produce thermoresponsive polymers is the random copolymerization of OEGAs and OEGMAs with different chain lengths.[49-53] The incorporation of catechol units, either as end or as side groups, into thermoresponsive polymers has been investigated with the aim of combining the thermoresponsiveness of the polymer with the anchoring/coordination capability of the catechol.[54,55] For example, thermoresponsive polymers based on the combination of di(ethylene glycol) ethyl ether acrylate and oligo(ethylene glycol) methyl ether acrylate ($OEGA_{480}$) with terminal catechol anchors have been synthesized for the surface modification of $TiO_2$ nanoparticles.[56] Recently, we reported the use of biscatechol-end-functional P(NIPAM) for the fabrication of thermoresponsive $Fe^{III}$ MPN capsules.[28] The brush PEG–CAF polymers developed in the present study differ from those reported in that the influence of the catechol on the thermal behavior of the polymer is also considered.

Computer simulation has provided insight into the dynamics of temperature transitions in water of thermally sensitive polymers such as P(NIPAM) and P(OEGMA).[57] The rationale for their phase behavior is that an alteration of the organization of water molecules (i.e., the hydration pattern) in the surrounding environment of the polymer occurs during phase transition. Concomitant with chain rearrangement on heating is a reduced level of water molecule structuring at the hydrophobic polymer–water interface. For P(OEGMA), at temperatures below the LCST, hydrophobic hydration around the side chain carbon atoms is achieved by cage-like water formations. Changes in the functional groups in the backbone and side chains alter the water arrangement around the polymers and therefore the overall entropy of the system.[48] It is noteworthy that cinnamic acid analogues have been applied as hydrophobic additives to alter the micellar characteristics of Triton X-100 assemblies, as well as to create superhydrophobic surfaces.[58,59] Our results strongly infer that caffeamide side chain functionality provides a dominant hydrophobic effect, thereby lowering the LCST. This likely

arises from both the hydrophobic aromatic ring, as well the unsaturated $C_2H_2$ functionality, contained in the cinnamoyl core. Dihydroxy and amide functionality, both of which can form hydrogen bonds with water, drive dissolution, however at temperatures below the LCST. The effect of the iBoc carbamate side product is indistinguishable from that of the caffeamide groups and given the consistently low levels produced in each polymer batch, it is unlikely to influence thermal behavior significantly.

The molar fraction of caffeamide groups in the brush PEG–CAF copolymers (**3a–3c** and replicate batch **7a–7c**) was the main factor influencing the LCST. As observed in Figure 1, the $T_{CP}$ could be incrementally increased from ~23 to ~35 and subsequently to ~45 °C by decreasing the CAF content from 50 to 40 and 30%, respectively. Importantly, these findings demonstrate that the incorporation of catechol units (CAFs) with $OEGMA_{500}$, which is known to yield biocompatible and stealthy polymers, allows the tuning of LCST to biologically relevant levels, i.e., ~37 °C.

We briefly investigated pH and salt effects using polymer **7b**, as these aspects can have a dramatic effect on the LCST behavior of amphiphilic copolymers (see Figure S25).[60] Since the acid dissociation constants ($pK_a$) for catechols are above pH 7 ($pK_{a1}$ = 9.25 and $pK_{a2}$ = 13.0)[61], at pH 10 the catechol groups are expected to be partly ionized. Since polymer-water interactions increase upon ionization, the hydrophilicity of the polymer is expected to increase under these conditions, thus increasing the phase transition temperature. At the same time, under caustic conditions catechol groups can also become oxidised, as indicated by the dark colour developed by the polymer solution during the test (see inset photo in Figure S25). In contrast, at low pH (<3) the sample became hazy at the onset temp (20 °C), indicating that the polymer chains were already aggregating. This is consistent with polymer–polymer hydrogen bonding interactions (between catechol hydroxyls and OEG groups) at low pH. Finally, the

observed reduction of phase transition temperature with added NaCl was consistent with theory, since ions are known to substantially alter the water structure around the polymer.

**Fabrication of Thermoresponsive $Fe^{III}$ MPN Capsules.** MPN systems prepared from commercially available phenolic molecules, such as tannic acid, have been shown to respond to various stimuli including pH, light, and redox potential;[62-64] however, engineering specific properties into the polymer building blocks is an attractive strategy for expanding the suite of stimulus-responsive MPNs.[28] In the present work, a synthetic strategy was devised to develop a thermoresponsive and tunable MPN system with an added functionality of operating within a biologically relevant temperature range. The currently engineered catechol-functionalized polymers, brush PEG–CAF copolymers **3a–3c**, were used as building blocks for the fabrication of $Fe^{III}$–based MPN capsules and for imparting thermoresponsive properties to the assembled MPN capsules. In particular, we examined the effect of the catechol content in the brush PEG–CAF copolymer building block on the shell thickness and temperature-induced dynamics of the capsules. MPN assembly was performed on PS-COOH (1.86 ± 0.03 μm), which were used as sacrificial templates, as previously described.[15,16] Removal of the PS-COOH templates was achieved via dissolution of the particles in THF (Figure 2a).

SEM and AFM images of the MPN capsules revealed the characteristic folds and creases of collapsed capsule structures in the air-dried state (Figure 2b). The shell thicknesses of the brush PEG–CAF–$Fe^{III}$ MPN capsules assembled using **3a–3c** were 12.2, 16.5, and 23.5 nm, respectively (Figure 2c and Table S13). As the OEGMA content in each brush PEG–CAF copolymer was maintained at the same $M_n$ value (~10 kDa, ~ 20 units of $OEGMA_{500}$), we could attribute the increase in shell thickness to the increase in the catechol content of the building block used for MPN assembly. This is expected as a higher number of catechol side groups lead to more interconnections and subsequently more polymer deposited onto the MPN network structure. A higher catechol content resulting in the formation of thicker films is

consistent with what we previously observed for PS-templated $Fe^{III}$ MPN capsules prepared using linear PEG–CAF building blocks with an equivalent PEG $M_n$.[27] The pH also affects the multivalent coordination bonding between catechol groups and $Fe^{III}$ ions during film formation.[16] The size of MPN capsules fabricated from the polymers **3b** and **3c** (with higher catechol contents) were found to decrease by 15.6 and 11.1%, respectively, when the pH was changed from 3 to 9 (Figure S26 and Table S14). A higher concentration of deprotonated catechol groups, along with a higher pH, promotes the formation of bis- and tris-coordination states, and therefore the formation of a more crosslinked and compact MPN.

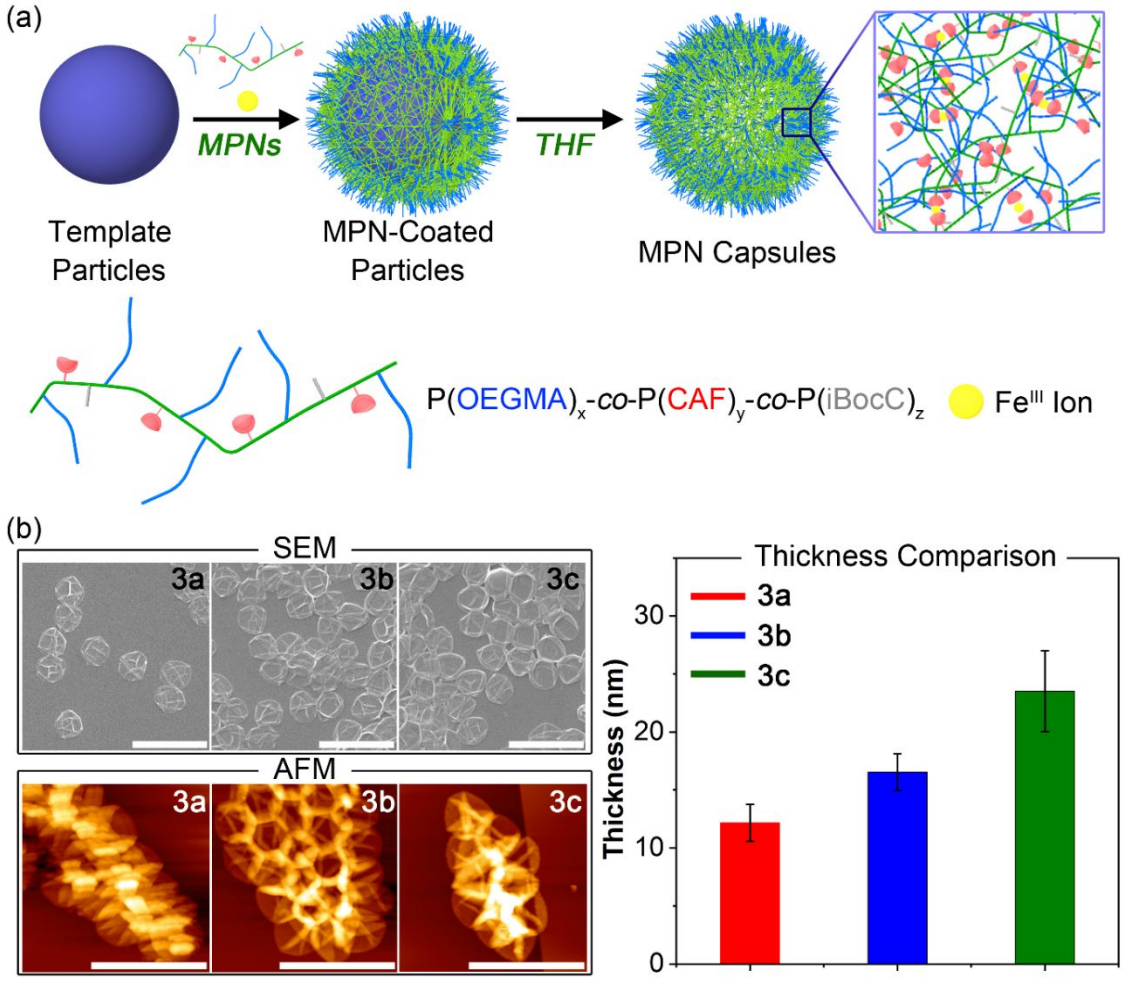


**Figure 2.** (a) Schematic illustration of the fabrication of brush PEG–CAF–$Fe^{III}$ MPN capsules. (b) SEM and AFM images of brush PEG–CAF–$Fe^{III}$ MPN capsules prepared from **3a–3c**. Scale bars are 5 μm. Shell thickness of brush PEG–CAF–$Fe^{III}$ MPN capsules as determined by AFM

height–distance graphs; data are shown as the mean ± standard deviation of five independent measurements for each capsule type.

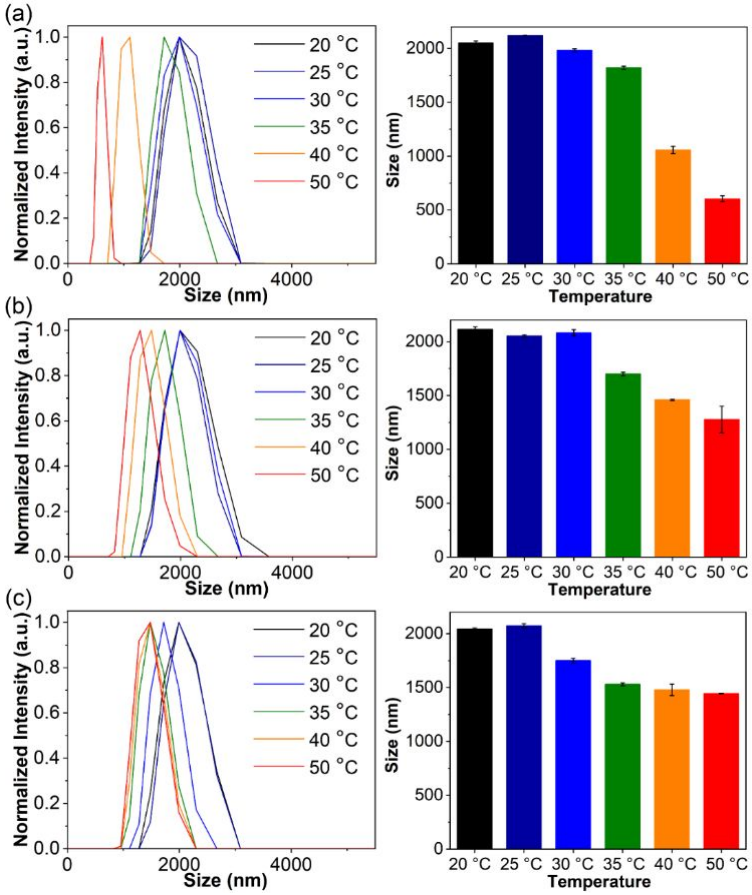


**Figure 3.** Temperature-activated size reduction of brush PEG–CAF–$Fe^{III}$ MPN capsules prepared from (a) **3a** (b) **3b**, and (c) **3c**, when heated from 20 to 50 °C. The hydrodynamic diameters, determined by DLS (intensity), are shown as the average ± standard deviation of three measurements.

The temperature-dependent size changes of the brush PEG–$Fe^{III}$ MPN capsules were monitored by DLS over the temperature range of 20–50 °C (Figure 3, Table S15). A reduction in capsule size in response to a temperature increase was observed for each capsule type. The size change in the capsules is reflective of compaction of polymer chains in the capsule wall, which occurs during the coil-to-globule phase transition, as the temperature is increased above the LCST. The extent of compaction is expected to be smaller for P(OEGMA)s compared to

P(NIPAM) because of the longer (brush) side chains. However, changes in size of the capsules were comparable to those observed for the previously reported α,ω-biscatechol-functionalized $P(NIPAM)_{364}$–$Fe^{III}$ MPN capsules.[28] Figure 3 shows the thermal response of the MPN capsules, namely the reduction in capsule diameter, in response to a temperature increase. When the temperature was increased from 25 to 50 °C, the diameter of the MPN capsules assembled from **3a–3c** decreased by 71.5, 39.6, and 30.3%, respectively. The size reduction in the average diameter of the MPN capsules was greatest for **3a**, which has the lowest quantity of catechol groups per chain. Conversely, polymer **3c**, with the highest amount of catechols, showed the least size reduction. On heating from 25 to 40 °C, the capsules composed of **3a** underwent a 50% reduction in size. The size contraction is likely to be affected by the number of catechol–$Fe^{III}$ interconnections formed, as well as the thickness of the capsule wall. It is likely that a higher catechol content creates a denser and less flexible MPN network structure for the capsule wall. An increase in the concentration of monomers in the initial mixture of a hydrogel is known to influence the cross-linking degree and the proportion of chain entanglements within a hydrogel structure, and therefore the viscoelastic properties and degree of swelling.[65] Specifically, a stiffer gel with a reduced ability to swell in water could also lead to a lower degree of contraction in response to an increase in temperature.

Capsules assembled using **3a** displayed the greatest incremental decrease in size on increasing the temperature from 35 to 40 °C, whereas for capsules assembled using **3b**, this occurred from 30 to 35 °C and for capsules prepared with **3c**, it occurred from 25 to 30 °C. Although the polymer structure (network vs free polymer) influences the thermal transition, it is reasonable to assume that the trends observed for the size reduction are directly associated with the thermal transitions of the brush PEG–CAF copolymers which make up the capsule wall. Minor deviations from measured cloud points (~45, ~35, and ~23°C for **3a**, **3b**, and **3c**, respectively) are also likely to arise from changes in the conditions of each measurement.

We reason that the hydrophobicity of the caffeamide functionality is responsible for the observed LCST trends. The observed LCST behavior of the MPN capsules also suggests that hydrogen bonding between the catechol dihydroxy groups and water molecules has relatively little effect on the phase transition as deprotonated catechol groups (which are not H-bonded) are involved in coordination states with $Fe^{III}$ in the MPN structure.

From a previous study,[28] the thermally induced size changes and the shell thickness of capsules were tuned by varying the molecular weight of the polymer. For the brush PEG–CAF copolymer building blocks developed in the present work, both the $M_n$ of the polymer and number of the catechol units could be customized, which could be both controlled by the feed ratio in the polymerization reaction. Furthermore, there was no requirement to alter the ratio of the catechol groups to the metal ions in the MPN process to affect the capsule wall thickness and thermoresponsiveness, which could also have a corresponding effect on the permeability of the capsules. Overall, the incorporated caffeamide functionalities offer two modes of application for the brush PEG−CAF copolymers: (i) they provide a means to tune the LCST of thermoresponsive P(OEGMA) to biologically relevant levels (~37 °C) and (ii) they can be used as phenolic ligands for MPN assembly, altogether affording MPN capsules with thermoresponsive properties.

**Mitigation of ROS.** P(OEGMA)-based polymers bearing short oligo(ethylene glycol) side chains are increasingly being considered as promising alternatives to P(NIPAM) for the fabrication of biocompatible and thermoresponsive biomaterials.[66] In the present work, we have demonstrated that caffeamide side chains can also be used to tune the LCST of P(OEGMA) to a biologically relevant temperature range (~37 °C). This opens the door for the design of biomedical smart materials. To this effect, we examined the effect of the polymers on cell viability and whether the polymers could reduce ROS levels in pathological conditions. In previous work, we developed a co-culture model comprised of fibroblasts (BJ-5ta) and

breast cancer cells (MCF-7), in which we found ROS levels to be elevated in the cancer cells of the co-culture.[36] ROS is understood to play a role in cellular communication between cancer cells and surrounding tumor-associated cells, such as fibroblasts.[67,68] Herein, we sought to determine, in this high ROS setting, whether the brush PEG–CAF copolymers can ameliorate oxidative stress. As a starting point, we evaluated the tolerance of the co-cultured cells to brush PEG–CAF polymers **3a–3c**, and the previously studied 4-arm, 10kDa linear PEG–CAF (**4a**).[27] Figure 4a shows the higher cell viability of the co-cultured MCF-7 and BJ-5ta cells when exposed to **4a** than 4-arm, 10kDa PEG-OH (Creative PEGworks), the latter being the starting material used to derive **4a**. Figure 4b shows that brush PEG–CAF **3a–3c** were also well tolerated by co-cultured cells after treatment for 24 h at all the concentrations examined (0.06–1.00 mg $mL^{-1}$). The cell viability, calculated with respect to untreated controls, was close to 100% for all the polymers studied. Among the brush PEG–CAF polymers, **3a** displayed a slightly lower cell viability than **3b** and **3c**. Overall, the cell tolerance of all polymers was high, with no apparent impact as a result of a higher proportion of catechol groups in the polymer or differing polymer structure (4-arm linear PEG vs brush PEG structure).

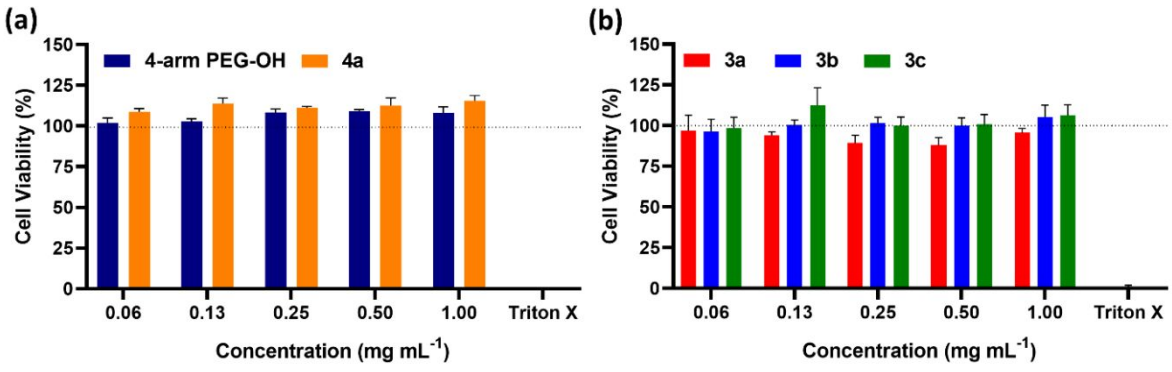


**Figure 4.** Cell viability (%) of co-cultured BJ-5ta and MCF-7 cells treated with (a) 4-arm, 10kDa linear PEG–CAF (**4a**) or 4-arm, 10kDa PEG-OH, or (b) brush PEG–CAF polymers **3a–3c**. Triton X (0.1%) in complete media was used as a positive control (cell viability equals 0%) (nontreated control group (no polymer, media only)). Data are presented for three experiments

and plotted as the mean ± standard error of the mean. Cell viability was assessed using Alamar Blue assay.

The attenuation of cellular ROS levels by the brush PEG–CAF polymers was evaluated on the developed co-culture model by monitoring ROS production using CellROX™ Deep Red Reagent for ROS staining. Under co-cultured conditions, MCF-7 cancer cells produced significant levels of ROS compared to co-cultured BJ-5ta fibroblasts, as well as mono-cultured MCF-7 cells. Therefore, the co-culture model is ideal to assess the antioxidant activity without the requirement of adding external oxidants or depleting antioxidant systems.[36,37] A preliminary study of comparing **4a** with brush polymers **3a**–**3c** did not show statistical difference in ROS generation between cells treated with polymers **3a**, **3b**, or **4a** (at 250 μg $mL^{-1}$) compared to the nontreated control group (Figure 5a). However, the brush PEG–CAF polymer **3c**, which contains the highest proportion of catechol (CAF) groups per polymer chain, could reduce the level of endogenous ROS in comparison with the nontreated control group. This trend was evident in both BJ-5ta cells and MCF-7 cells in the co-culture, the latter having higher levels of ROS (Figure 5b).

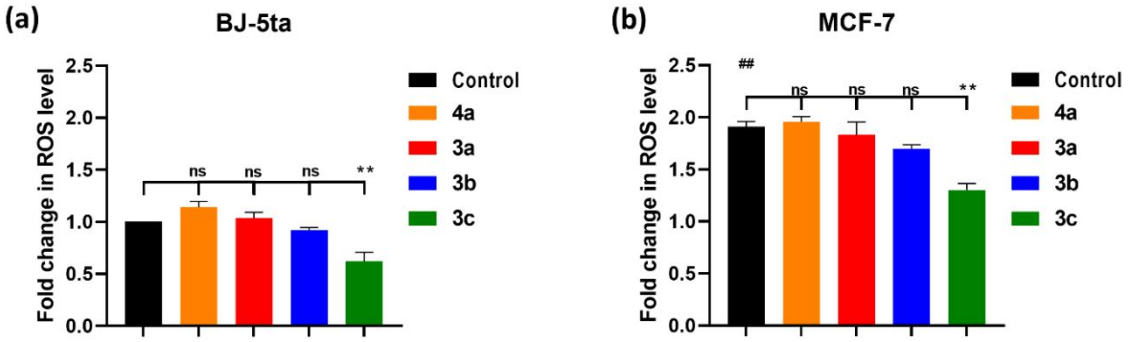


**Figure 5.** Fold change in ROS levels (relative to co-cultured fibroblasts in control groups) for (a) co-cultured BJ-5ta fibroblasts and (b) MCF-7 breast cancer cells when exposed to brush polymers **3a–3c** or 4-arm, 10kDa linear PEG–CAF **4a** at 250 μg $mL^{-1}$ for 24 h, in comparison with corresponding cells without any treatment (control). Data are presented for three independent experiments ($N = 3$). Statistical significance of difference from the control groups

(BJ-5ta in (a) or MCF-7 in (b)) was determined by a matched ANOVA with Dunnett's multiple comparisons post-hoc test; **, $p < 0.01$; ns, not significant. Statistical significance of difference between co-cultured fibroblasts and co-cultured breast cancer cells in the control group was acquired from a paired *t*-test; ##, $p < 0.01$. Error bars represent standard error of the mean.

Subsequently, we examined the ability of polymers to protect cells from exogenous oxidative stress, with the addition of *tert*-butyl hydroperoxide (TBHP). To identify the appropriate concentrations for subsequent ROS mitigation tests, the co-cultured BJ-5ta fibroblasts and MCF-7 breast cancer cells were exposed for 24 h to **4a** (500 and 250 μg $mL^{-1}$) or 4-arm, 10kDa PEG-OH (500 μg $mL^{-1}$), followed by TBHP exposure for 1 h (Figure S27). Cells without any treatment (control) or treated with TBHP only were also examined. A significant reduction in ROS levels was observed following exposure to **4a** at both concentrations relative to the ROS levels for cells treated with TBHP only or TBHP + 4-arm PEG-OH. Thus, the minimum concentration of 250 μg $mL^{-1}$ was deemed appropriate for further testing.

Based on the abilities of **3c** to reduce endogenous ROS in the co-culture (Figure 5) and of **4a** to reduce exogenous ROS (Figure S27), a comparative test of exogenous ROS reduction was performed using **4a** and **3c**. Figure 6 shows changes in the ROS level for co-cultured BJ-5ta fibroblasts and MCF-7 breast cancer cells when exposed to linear PEG–CAF **4a** or brush PEG–CAF **3c** at 250 μg $mL^{-1}$ for 24 h, followed by TBHP treatment. A significant reduction in ROS level was observed in the brush PEG–CAF **3c** group relative to the nontreated control group. This result was consistent with the reduction in endogenous ROS levels observed in both cell lines upon introduction of **3c**. Altogether, these results indicate that a high concentration of catechols in the brush PEG–CAF copolymers (i.e., 50% vs OEGMA) enhances ROS scavenging.

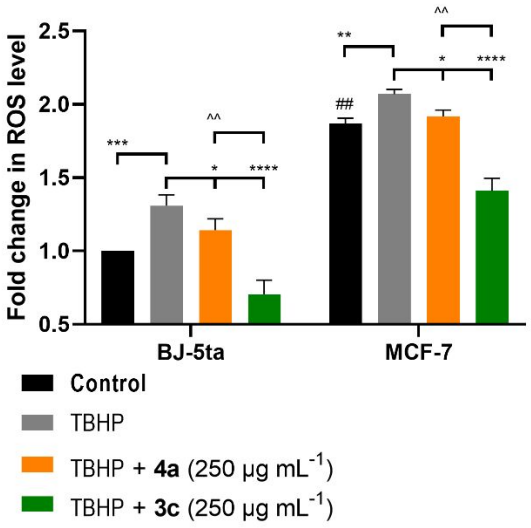


**Figure 6.** Fold change in ROS levels of co-cultured BJ-5ta fibroblasts and MCF-7 breast cancer cells when exposed to 4-arm, 10kDa linear PEG–CAF **4a** or brush PEG–CAF polymer **3c** at 250 μg $mL^{-1}$ for 24 h followed by TBHP treatment (100 μM) for 1 h. Cells without any treatment (control) or treated with TBHP only (TBHP) were also examined. Data are presented for three independent experiments ($N$ = 3). Statistical significance difference for the TBHP-treated cells (BJ-5ta or MCF-7) was determined by a matched two-way ANOVA with Dunnett's multiple comparisons post-hoc test; *, $p < 0.05$; ***, $p < 0.001$; ****, $p < 0.0001$; ns, not significant. Statistical significance difference between TBHP + **4a** and TBHP + **3c** groups (in either BJ-5ta or MCF-7 cells) was determined by a matched two-way ANOVA with Sidak's multiple comparisons post-hoc test; ^^, $p < 0.01$. Statistical significance between co-cultured fibroblasts and co-cultured breast cancer cells in the control group was acquired from a paired $t$-test; ##, $p < 0.01$. Error bars represent standard error of the mean.

## CONCLUSIONS

A library of brush PEG–CAF polymers with varying catechol contents were synthesized by conjugation of the acyl-protected and activated intermediate, caffeic acid carbonic anhydride, to amine functional P($OEGMA_{500}$), followed by catechol deprotection. The polymers were synthesized reproducibly and displayed LCST behavior, as confirmed via $T_{CP}$ measurements.

The molar fraction of caffeamide (CAF) groups was the key factor influencing the thermal transition, as a result of caffeoyl hydrophobicity, allowing the tuning of the LCST to biologically relevant levels (i.e., 25–40 °C). Using the thermoresponsive building blocks, thermoresponsive $Fe^{III}$ MPN capsules were prepared, with increasing shell thickness as the CAF content of the building block was increased. The MPN capsules exhibited a contraction in capsule size upon heating from 20 to 50 °C, with the extent of contraction dependent on the CAF content of the building block.

It was also demonstrated that the brush PEG–CAF building block containing the highest amount of CAF units (50%) could attenuate ROS levels both in a co-culture model of naturally elevated ROS levels and when exposed to exogenous oxidants. Overall, the tuning of LCST of P(OEGMA) to a biologically relevant temperature range, combined with ability of CAF groups to reduce ROS levels suggest that the caffeamide-rich polymers engineered herein may potentially be used as therapeutic drug carriers, especially in disease settings where ROS levels are elevated.

## ASSOCIATED CONTENT

**Supporting Information.** Representative high-content fluorescence images used for probing cellular ROS levels; tabulated details of synthesis and polymer characteristics for all brush PEG–CAF copolymers and prepolymers and associated $^1$H NMR and GPC analyses; absorption spectrum of caffeic acid in water; fluorescence spectrum of polymer **3c** in water vs caffeic acid in water; transmittance–temperature curve of **7b** vs salt and pH; temperature and pH induced size changes of MPN capsules as measured by DLS; AFM shell thickness measurements; additional ROS generation detection testing with TBHP. This material is available free of charge via the Internet at http://pub.acs.org.

## AUTHOR INFORMATION

**Corresponding Author**

*E-mail: john.f.quinn@monash.edu

**Author Contributions**

The manuscript was written through contributions of all authors. All authors have given approval to the final version of the manuscript.

**Notes**

The authors declare no competing financial interest.

ACKNOWLEDGMENTS

This research was funded by the Australian Research Council through the Discovery Project (DP200100713) scheme. F.C. acknowledges the award of a National Health and Medical Research Council Senior Principal Research Fellowship (GNT1135806). J.F.Q. acknowledges the receipt of a Future Fellowship (FT170100144) from the ARC. This work was performed in part at the Materials Characterization and Fabrication Platform (MCFP) at the University of Melbourne and the Victorian Node of the Australian National Fabrication Facility (ANFF).

REFERENCES

1. Wu, D.; Zhou, J. J.; Creyer, M. N.; Yim, W.; Chen, Z.; Messersmith, P. B.; Jokerst, J. V. Phenolic-Enabled Nanotechnology: Versatile Particle Engineering for Biomedicine. *Chem. Soc. Rev.* **2021**, *50*, 4432-4483.

2. Chen, G. C.; Yi, Z.; Chen, X. Y.; Ma, X. M.; Su, W.; Li, X. D. Polyphenol Nanoparticles from Commonly Consumed Tea for Scavenging Free Radicals, Stabilizing Pickering Emulsions, and Inhibiting Cancer Cells. *ACS Appl. Nano Mater.* **2021**, *4*, 652-665.

3. Gao, X. Z.; Xu, Z. J.; Liu, G. T.; Wu, J. Polyphenols as a Versatile Component in Tissue Engineering. *Acta Biomater.* **2021**, *119*, 57-74.

4. Mustafa, S. K.; Oyouni, A.; Aljohani, M. M. H.; Ahmad, M. A. Polyphenols More Than an Antioxidant: Role and Scope. *J. Pure Appl. Microbiol.* **2020**, *14*, 47-61.

5. Magrone, T.; Magrone, M.; Russo, M. A.; Jirillo, E. Recent Advances on the Anti-Inflammatory and Antioxidant Properties of Red Grape Polyphenols: In Vitro and In Vivo Studies. *Antioxidants* **2020**, *9*, 35. doi: 10.3390/antiox9010035

6. Patil, N.; Jerome, C.; Detrembleur, C. Recent Advances in the Synthesis of Catechol-Derived (Bio)Polymers for Applications in Energy Storage and Environment. *Prog. Polym. Sci.* **2018**, *82*, 34-91.

7. Son, S.; Lewis, B. A. Free Radical Scavenging and Antioxidative Activity of Caffeic Acid Amide and Ester Analogues: Structure–Activity Relationship. *J. Agric. Food Chem.* **2002**, *50*, 468-472.

8. Li, A. N.; Li, S.; Zhang, Y. J.; Xu, X. R.; Chen, Y. M.; Li, H. B. Resources and Biological Activities of Natural Polyphenols. *Nutrients* **2014**, *6*, 6020-6047.

9. Quideau, S.; Deffieux, D.; Douat-Casassus, C.; Pouysegu, L. Plant Polyphenols: Chemical Properties, Biological Activities, and Synthesis. *Angew. Chem. Int. Ed.* **2011**, *50*, 586-621.

10. Waite, J. H.; Tanzer, M. L. Polyphenolic Substance of *Mytilus edulis*: Novel Adhesive Containing L-Dopa and Hydroxyproline. *Science* **1981**, *212*, 1038-1040.

11. Yu, M. E.; Hwang, J. Y.; Deming, T. J. Role of L-3,4-Dihydroxyphenylalanine in Mussel Adhesive Proteins. *J. Am. Chem. Soc.* **1999**, *121*, 5825-5826.

12. Lee, H.; Scherer, N. F.; Messersmith, P. B. Single-Molecule Mechanics of Mussel Adhesion. *Proc. Natl. Acad. Sci. U. S. A.* **2006**, *103*, 12999-13003.

13. Wu, J.; Omene, C.; Karkoszka, J.; Bosland, M.; Eckard, J.; Klein, C. B.; Frenkel, K. Caffeic Acid Phenethyl Ester (CAPE), Derived from a Honeybee Product Propolis, Exhibits a Diversity of Anti-Tumor Effects in Pre-Clinical Models of Human Breast Cancer. *Cancer Lett.* **2011**, *308*, 43-53.

14. Kim, J.; Lee, K.; Nam, Y. S. Metal-Polyphenol Complexes as Versatile Building Blocks for Functional Biomaterials. *Biotechnol. Bioprocess Eng.* **2021**, *26*, 689-707.

15. Ejima, H.; Richardson, J. J.; Caruso, F. Metal-Phenolic Networks as a Versatile Platform to Engineer Nanomaterials and Biointerfaces. *Nano Today* **2017**, *12*, 136-148.

16. Ejima, H.; Richardson, J. J.; Liang, K.; Best, J. P.; van Koeverden, M. P.; Such, G. K.; Cui, J. W.; Caruso, F. One-Step Assembly of Coordination Complexes for Versatile Film and Particle Engineering. *Science* **2013**, *341*, 154-157.

17. Ju, Y.; Cortez-Jugo, C.; Chen, J. Q.; Wang, T. Y.; Mitchell, A. J.; Tsantikos, E.; Bertleff-Zieschang, N.; Lin, Y. W.; Song, J. Y.; Cheng, Y. Z.; Mettu, S.; Rahim, M. A.; Pan, S. J.; Yun, G. W.; Hibbs, M. L.; Yeo, L. Y.; Hagemeyer, C. E.; Caruso, F. Engineering of Nebulized Metal–Phenolic Capsules for Controlled Pulmonary Deposition. *Adv. Sci.* **2020**, *7*, 1902650. doi: 10.1002/advs.201902650

18. Guo, J. L.; Ping, Y.; Ejima, H.; Alt, K.; Meissner, M.; Richardson, J. J.; Yan, Y.; Peter, K.; von Elverfeldt, D.; Hagemeyer, C. E.; Caruso, F. Engineering Multifunctional Capsules through the Assembly of Metal-Phenolic Networks. *Angew. Chem. Int. Ed.* **2014**, *53*, 5546-5551.

19. Ju, Y.; Cui, J. W.; Mullner, M.; Suma, T.; Hu, M.; Caruso, F. Engineering Low-Fouling and pH-Degradable Capsules through the Assembly of Metal-Phenolic Networks. *Biomacromolecules* **2015**, *16*, 807-814.

20. Krogsgaard, M.; Nue, V.; Birkedal, H. Mussel-Inspired Materials: Self-Healing through Coordination Chemistry. *Chem. Euro. J.* **2016**, *22*, 844-857.

21. Faure, E.; Falentin-Daudre, C.; Jerome, C.; Lyskawa, J.; Fournier, D.; Woisel, P.; Detrembleur, C. Catechols as Versatile Platforms in Polymer Chemistry. *Prog. Polym. Sci.* **2013**, *38*, 236-270.

22. Zhang, H.; Zhao, T. Y.; Newland, B.; Liu, W. G.; Wang, W.; Wang, W. X. Catechol Functionalized Hyperbranched Polymers as Biomedical Materials. *Prog. Polym. Sci.* **2018**, *78*, 47-55.

23. Xue, X.; Pasparakis, G.; Halliday, N.; Winzer, K.; Howdle, S. M.; Cramphorn, C. J.; Cameron, N. R.; Gardner, P. M.; Davis, B. G.; Fernandez-Trillo, F.; Alexander, C. Synthetic Polymers for Simultaneous Bacterial Sequestration and Quorum Sense Interference. *Angew. Chem. Int. Ed.* **2011**, *50*, 9852-9856.

24. Shin, E.; Lim, C.; Kang, U. J.; Kim, M.; Park, J.; Kim, D.; Choi, W.; Hong, J.; Baig, C.; Lee, D. W.; Kim, B. S. Mussel-Inspired Copolyether Loop with Superior Antifouling Behavior. *Macromolecules* **2020**, *53*, 3551-3562.

25. Gan, D. L.; Xu, T.; Xing, W. S.; Ge, X.; Fang, L. M.; Wang, K. F.; Ren, F. Z.; Lu, X. Mussel-Inspired Contact-Active Antibacterial Hydrogel with High Cell Affinity, Toughness, and Recoverability. *Adv. Funct. Mater.* **2019**, *29*, 1805964. doi: 10.1002/adfm.201805964.

26. Yang, B.; Lv, Y.; Zhu, J. Y.; Han, Y. T.; Jia, H. Z.; Chen, W. H.; Feng, J.; Zhang, X. Z.; Zhuo, R. X. A pH-Responsive Drug Nanovehicle Constructed by Reversible Attachment

of Cholesterol to PEGylated Poly(L-lysine) Via Catechol–Boronic Acid Ester Formation. *Acta Biomater.* **2014**, *10*, 3686-3695.

27. Kim, C. J.; Ercole, F.; Ju, Y.; Pan, S. J.; Chen, J. Q.; Qu, Y.; Quinn, J. F.; Caruso, F. Synthesis of Customizable Macromolecular Conjugates as Building Blocks for Engineering Metal–Phenolic Network Capsules with Tailorable Properties. *Chem. Mater.* **2021**, *33*, 8477-8488.

28. Kim, C. J.; Ercole, F.; Chen, J. Q.; Pan, S. J.; Ju, Y.; Quinn, J. F.; Caruso, F. Macromolecular Engineering of Thermoresponsive Metal–Phenolic Networks. *J. Am. Chem. Soc.* **2021**, *144*, 503-514.

29. Rahim, M. A.; Kristufek, S. L.; Pan, S. J.; Richardson, J. J.; Caruso, F. Phenolic Building Blocks for the Assembly of Functional Materials. *Angew. Chem. Int. Ed.* **2019**, *58*, 1904-1927.

30. Su, J.; Chen, F.; Cryns, V. L.; Messersmith, P. B. Catechol Polymers for pH-Responsive, Targeted Drug Delivery to Cancer Cells. *J. Am. Chem. Soc.* **2011**, *133*, 11850-11853.

31. Barros, N. R.; Chen, Y.; Hosseini, V.; Wang, W. Y.; Nasiri, R.; Mahmoodi, M.; Yalcintas, E. P.; Haghniaz, R.; Mecwan, M. M.; Karamikamkar, S.; Dai, W.; Sarabi, S. A.; Falcone, N.; Young, P.; Zhu, Y. Z.; Sun, W. J.; Zhang, S. M.; Lee, J. M.; Lee, K.; Ahadian, S.; Dokmeci, M. R.; Khademhosseini, A.; Kim, H. J. Recent Developments in Mussel-Inspired Materials for Biomedical Applications. *Biomater. Sci.* **2021**, *9*, 6653-6672.

32. Lin, Y. H.; Yan, Y. J. Biosynthesis of Caffeic Acid in *Escherichia coli* Using Its Endogenous Hydroxylase Complex. *Microb. Cell Fact.* **2012**, *11*, 42. doi: 10.1186/1475-2859-11-42.

33. Yoshimoto, M.; Kurata-Azuma, R.; Fujii, M.; Hou, D. X.; Ikeda, K.; Yoshidome, T.; Osako, M. Enzymatic Production of Caffeic Acid by Koji from Plant Resources Containing Caffeoylquinic Acid Derivatives. *Biosci. Biotechnol. Biochem.* **2005**, *69*, 1777-1781.

34. Rajan, P.; Vedernikova, I.; Cos, P.; Vanden Berghe, D.; Augustyns, K.; Haemers, A. Synthesis and Evaluation of Caffeic Acid Amides as Antioxidants. *Bioorg. Med. Chem. Lett.* **2001**, *11*, 215-217.

35. Shahidi, F.; Janitha, P. K.; Wanasundara, P. D. Phenolic Antioxidants. *Crit. Rev. Food Sci. Nutr.* **1992**, *32*, 67-103.

36. Dao, N. V.; Ercole, F.; Urquhart, M. C.; Kaminskas, L. M.; Nowell, C. J.; Davis, T. P.; Sloan, E. K.; Whittaker, M. R.; Quinn, J. F. Trisulfide Linked Cholesteryl PEG Conjugate Attenuates Intracellular ROS and Collagen-1 Production in a Breast Cancer Co-Culture Model. *Biomater. Sci.* **2021**, *9*, 835-846.

37. Dao, N. V.; Ercole, F.; Li, Y. H.; Davis, T. P.; Kaminskas, L. M.; Sloan, E. K.; Quinn, J. F.; Whittaker, M. R. Nitroxide-Functional PEGylated Nanostars Arrest Cellular Oxidative Stress and Exhibit Preferential Accumulation in Co-Cultured Breast Cancer Cells. *J. Mater. Chem. B* **2021**, *9*, 7805-7820.

38. Lew, M. Good Statistical Practice in Pharmacology. Problem 2. *Br. J. Pharmacol.* **2007**, *152*, 299-303.

39. Chen, F. M. F.; Lee, Y.; Steinauer, R.; Benoiton, N. L. Mixed Anhydrides in Peptide-Synthesis. A Study of Urethane Formation with a Contribution on Minimization of Racemization. *Can. J. Chem.* **1987**, *65*, 613-618.

40. Chrostowski, P. C.; Dietrich, A. M.; Suffet, I. H. Ozone and Oxygen Induced Oxidative Coupling of Aqueous Phenolics. *Water Res.* **1983**, *17*, 1627-1633.

41. Xiang, Y.; Duan, L.; Ma, Q.; Lv, Z.; Ruohua, Z.; Zhang, Z. Fluorescence spectroscopy and molecular simulation on the interaction of caffeic acid with human serum albumin. Luminescence, **2016**, *31*, 1496-1502.

42. Zhu, H. P.; Zhao, H. W.; Zhang, Z. X.; Wang, W. F.; Yao, S. D. Laser flash photolysis study on antioxidant properties of hydroxycinnamic acid derivatives. *Radiat. Environ. Biophys.*, **2006**, *45*, 73–77.

43. Tavagnacco, L.; Zaccarelli, E.; Chiessi, E. On the Molecular Origin of the Cooperative Coil-to-Globule Transition of Poly(*N*-isopropylacrylamide) in Water. *Phys. Chem. Chem. Phys.* **2018**, *20*, 9997-10010.

44. Osvath, Z.; Ivan, B. The Dependence of the Cloud Point, Clearing Point, and Hysteresis of Poly(*N*-isopropylacrylamide) on Experimental Conditions: The Need for Standardization of Thermoresponsive Transition Determinations. *Macromol. Chem. Phys.* **2017**, *218*, 1600470.

45. Schild, H. G. Poly(*N*-isopropylacrylamide): Experiment, Theory and Application. *Prog. Polym. Sci.* **1992**, *17*, 163-249.

46. Halperin, A.; Kroger, M.; Winnik, F. M. Poly(*N*-isopropylacrylamide) Phase Diagrams: Fifty Years of Research. *Angew. Chem. Int. Ed.* **2015**, *54*, 15342-15367.

47. Ishizone, T.; Seki, A.; Hagiwara, M.; Han, S.; Yokoyama, H.; Oyane, A.; Deffieux, A.; Carlotti, S. Anionic Polymerizations of Oligo(Ethylene glycol) Alkyl Ether Methacrylates: Effect of Side Chain Length and ω-Alkyl Group of Side Chain on Cloud Point in Water. *Macromolecules* **2008**, *41*, 2963-2967.

48. Becer, C. R.; Hahn, S.; Fijten, M. W. M.; Thijs, H. M. L.; Hoogenboom, R.; Schubert, U. S. Libraries of Methacrylic Acid and Oligo(Ethylene glycol) Methacrylate Copolymers with LCST Behavior. *J. Polym. Sci., Part A: Polym. Chem.* **2008**, *46*, 7138-7147.

49. Lutz, J.-F.; Hoth, A. Preparation of Ideal PEG Analogues with a Tunable Thermosensitivity by Controlled Radical Copolymerization of 2-(2-Methoxyethoxy)ethyl Methacrylate and Oligo(Ethylene glycol) Methacrylate. *Macromolecules* **2006**, *39*, 893-896.

50. Badi, N. Non-Linear PEG-Based Thermoresponsive Polymer Systems. *Prog. Polym. Sci.* **2017**, *66*, 54-79.

51. Lutz, J.-F.; Hoth, A.; Schade, K. Design of Oligo(Ethylene glycol)-Based Thermoresponsive Polymers: An Optimization Study. *Des. Monomers Polym.* **2009**, *12*, 343-353.

52. Fechler, N.; Badi, N.; Schade, K.; Pfeifer, S.; Lutz, J. F. Thermogelation of PEG-Based Macromolecules of Controlled Architecture. *Macromolecules* **2009**, *42*, 33-36.

53. Lutz, J. F. Thermo-Switchable Materials Prepared Using the OEGMA-Platform. *Adv. Mater.* **2011**, *23*, 2237-2243.

54. Zhao, Y. H.; Wu, Y.; Wang, L.; Zhang, M. M.; Chen, X.; Liu, M. J.; Fan, J.; Liu, J. Q.; Zhou, F.; Wang, Z. K. Bio-Inspired Reversible Underwater Adhesive. *Nat. Commun.* **2017**, *8*, 2218. doi: 10.1038/s41467-017-02387-2.

55. Duan, H. C.; Yang, Y.; Lu, J. H.; Lu, C. L. Mussel-Inspired Construction of Thermo-Responsive Double-Hydrophilic Diblock Copolymers-Decorated Reduced Graphene Oxide as Effective Catalyst Supports for Highly Dispersed Superfine Pd Nanoparticles. *Nanoscale* **2018**, *10*, 12487-12496.

56. Wang, D. H.; Guo, S. T.; Zhang, Q.; Wilson, P.; Haddleton, D. M. Mussel-Inspired Thermoresponsive Polymers with a Tunable LCST by Cu(0)-LRP for the Construction of Smart $TiO_2$ Nanocomposites. *Polym. Chem.* **2017**, *8*, 3679-3688.

57. Dalgakiran, E.; Tatlipinar, H. The Role of Hydrophobic Hydration in the LCST Behaviour of $POEGMA_{300}$ by All-Atom Molecular Dynamics Simulations. *Phys. Chem. Chem. Phys.* **2018**, *20*, 15389-15399.

58. Razayi, S. M. R.; Oh, J.; Sett, S.; Feng, L. Z.; Yan, X.; Hoque, M. J.; Liu, A. H.; Haasch, R. T.; Masoomi, M.; Bagheri, R.; Miljkovic, N. Superhydrophobic Surfaces Made from Naturally Derived Hydrophobic Materials. *ACS Sustainable Chem. Eng.* **2017**, *5*, 11362-11370.

59. Patel, V.; Ray, D.; Aswal, V. K.; Bahadur, P. Triton X-100 Micelles Modulated by Solubilized Cinnamic Acid Analogues: The pH Dependant Micellar Growth. *Colloids Surf., A* **2014**, *450*, 106-114.

60. Yin X., and Sto1ver H.D.H. Thermosensitive and pH-Sensitive Polymers Based on Maleic Anhydride Copolymers *Macromolecules* **2002**, *35*, 10178-10181.

61. Schweigert, N.; Zehnder A. J.; Eggen R. I. Chemical properties of catechols and their molecular modes of toxic action in cells, from microorganisms to mammals. *Environ. Microbiol.* **2001**, *3*, 81-91.

62. Cherepanov, P. V.; Rahim, M. A.; Bertleff-Zieschang, N.; Sayeed, M. A.; O'Mullane, A. P.; Moulton, S. E.; Caruso, F. Electrochemical Behavior and Redox-Dependent Disassembly of Gallic Acid/$Fe^{III}$ Metal–Phenolic Networks. *ACS Appl. Mater. Interfaces* **2018**, *10*, 5828-5834.

63. Chen, J.; Pan, S.; Zhou, J.; Zhong, Q.-Z.; Qu, Y.; Richardson, J. J.; Caruso, F. Programmable Permeability of Metal–Phenolic Network Microcapsules. *Chem. Mater.* **2020**, *32*, 6975-6982.

64. Lin, G.; Richardson, J. J.; Ahmed, H.; Besford, Q. A.; Christofferson, A. J.; Beyer, S.; Lin, Z.; Rezk, A. R.; Savioli, M.; Zhou, J.; McConville, C. F.; Cortez-Jugo, C.; Yeo, L. Y.; Caruso, F. Programmable Phototaxis of Metal–Phenolic Particle Microswimmers. *Adv. Mater.* **2021**, *33*, 2006177. doi: 10.1002/adma.202006177.

65. Orakdogen, N.; Okay, O. Effect of Initial Monomer Concentration on the Equilibrium Swelling and Elasticity of Hydrogels. *Eur. Polym. J.* **2006**, *42*, 955-960.

66. Badi, N.; Lutz, J.-F. PEG-Based Thermogels: Applicability in Physiological Media. *J. Controlled Release* **2009**, *140*, 224-229.

67. Storz, P. Reactive Oxygen Species in Tumor Progression. *Front. Biosci.* **2005**, *10*, 1881-96.

68. Nishikawa, M. Reactive Oxygen Species in Tumor Metastasis. *Cancer Lett.* **2008**, *266*, 53-59.

Table of Contents graphic